

Enhanced Charge Transfer from Coinage Metal Doped InP Quantum Dots

Forrest W. Eagle, Samantha Harvey, Ryan Beck, Xiaosong Li, Daniel R. Gamelin, and Brandi M. Cossairt*



Cite This: *ACS Nanosci. Au* 2023, 3, 451–461



Read Online

ACCESS |

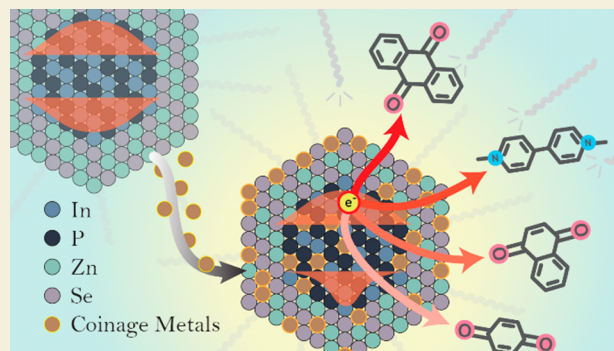
Metrics & More

Article Recommendations

Supporting Information

ABSTRACT: This paper describes coinage-metal-doped InP quantum dots (QDs) as a platform for enhanced electron transfer to molecular acceptors relative to undoped QDs. A synthetic strategy is developed to prepare doped InP/ZnSe QDs. First-principles DFT calculations show that Ag^+ and Cu^+ dopants localize photoexcited holes while leaving electrons delocalized. This charge carrier wave function modulation is leveraged to enhance electron transfer to molecular acceptors by up to an order of magnitude. Examination of photoluminescence quenching data suggests that larger electron acceptors, such as anthraquinone and methyl viologen, bind to the QD surface in two ways: by direct adsorption to the surface and by adsorption following displacement of a weakly bound surface cation-ligand complex. Reactions with larger acceptors show the greatest increases in electron transfer between doped and undoped quantum dots, while smaller acceptors show smaller enhancements. Specifically, benzoquinone shows the smallest, followed by naphthoquinone and then methyl viologen and anthraquinone. These results demonstrate the benefits of dopant-induced excited-state carrier localization on photoinduced charge transfer and highlight design principles for improved implementation of quantum dots in photoredox catalysis.

KEYWORDS: quantum dot, indium phosphide, charge transfer, donor–acceptor, doping, coinage metal



INTRODUCTION

With the global demand for value-added chemical products increasing each year, new catalytic materials must be developed to improve process efficiency. Many current processes require the use of intense reaction conditions, such as a high pressure or temperature. Solar powered catalysts offer an attractive alternative or supplement to current processes. Efficient photocatalytic materials typically require three characteristics: high extinction coefficients, high photostability, and long-lived photoexcited states. Many current photocatalysts are based on rare metals such as rhodium or iridium, which can have high turnover numbers depending on the specific reaction.^{1,2} However, these compounds often do not have large absorption cross sections at $\lambda > 400$ nm, which results in underutilization of the solar spectrum.

Quantum dots (QDs) intrinsically have large, tunable extinction coefficients,³ which can be further enhanced by adding inorganic shells on their surfaces.⁴ Inorganic shells also improve quantum dot stability^{5–7} and passivate surface states that serve as charge carrier traps.^{8,9} By shelling using a traditional Type-1 heterostructure, charge carriers are highly localized to the core of the quantum dot,¹⁰ making charge transfer difficult due to the energetic barrier for tunneling. This, along with the relatively short excited-state lifetimes

found in traditional III–V and II–VI quantum dots (QDs) (<50 ns),^{11,12} makes them a poor platform for photoredox catalysis. Despite these issues, quantum dots have been shown to perform a catalogue of photochemical reactions, such as hydrogen evolution and organic C–C, C–O, and C–N bond making and breaking reactions. However, photocatalytic organic reactions typically occur through optically dark triplet-like excitonic states and hydrogen evolution often requires cocatalysts.^{13–16}

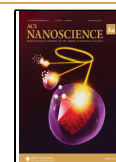
With the idea of designing improved quantum dot photocatalysts, the observation that coinage metal dopants, such as copper, enhance charge-carrier lifetimes by over an order of magnitude is notable.^{17–20} This increase in is found in II–VI nanocrystals (and InP) as these dopants introduce hole trap states, where photoexcited electrons can recombine with trapped holes.^{21,22}

Received: June 23, 2023

Revised: August 24, 2023

Accepted: August 25, 2023

Published: September 7, 2023



Recent work in our lab has demonstrated the introduction of copper dopants into III–V quantum dots, along with the spectroscopic examination of the charge carriers, finding that the photogenerated hole rapidly localizes to the copper site before other trapping processes occur similar to what has been observed in II–VI systems.^{17,19–21,23,24} Previous theoretical work has investigated the electronic structure of Cu⁺ and Ag⁺ doped CdSe quantum dots, showing that the emissive excited state consists of a delocalized electron and a hole localized at the copper dopant, with broad photoluminescence spectra arising due to vibronic coupling.^{18,19} Theoretical work on Cu⁺-doped InP suggested that their electronic structure is strongly dependent on ligand coating and other effects such as self-compensation.²⁵

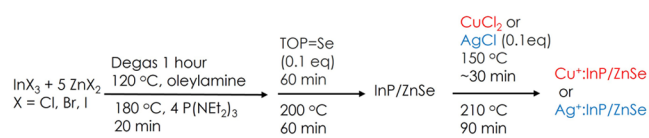
Here we prepare a series of Cu⁺- and Ag⁺-doped InP QDs, each shelled with a monolayer of ZnSe. The physical and electronic structures are studied by means of electron microscopy, elemental analysis, powder X-ray diffraction, steady-state and time-resolved optical spectroscopy, and first-principles DFT calculations. Using a combination of static and dynamic fluorescence quenching experiments and transient-absorption spectroscopy, we demonstrate the enhancement of electron transfer upon doping InP quantum dots with Cu⁺ and Ag⁺. We also show that this enhancement is strongly dependent on the electron acceptor's mechanism of adsorption to the quantum dot surface. Smaller acceptors show the highest rates of electron transfer from doped QDs but also lower enhancement when comparing doped versus undoped QDs due to the ability to adsorb directly to the surface of the quantum dot without requiring a dissociation step.

RESULTS AND DISCUSSION

Synthesis and Characterization of Doped InP/ZnSe QDs

A general synthesis of core/shell InP/ZnSe QDs was adapted from ref 23 (Scheme 1). In brief, 1 equiv of indium halide,

Scheme 1. General Synthesis of Coinage Metal Doped InP/ZnSe Core/Shell QDs



approximately 5 equiv of ZnCl₂, and an excess of dried and distilled oleylamine were combined, degassed at 120 °C, and heated to 180 °C. Approximately 4 equiv of tris-diethylaminophosphine was then rapidly injected. After a fixed period of time (see the Supporting Information), 1 M TOP=Se was slowly injected. After an hour, the reaction temperature was increased to 200 °C and held for an additional hour. Doped samples were synthesized following the same method as above with a few notable changes. After 120 min of reaction with TOP=Se, the temperature was decreased to 150 °C and a solution of 0.1 equiv of copper(II) chloride (CuCl₂) or silver(I) chloride (AgCl) was slowly injected (1 mL at 2 mL/h). After complete addition, the temperature was increased to 210 °C and held there for 1.5 h. In all cases, purification was achieved by 5 repeated cycles of precipitation and redissolution with anhydrous ethanol and toluene, respectively.

Using this method, ICP-OES data show InP/ZnSe QDs with 11% Cu and 6% Ag (reported as cation mole fraction, Table

S1). The QDs show little change in structure as determined by powder X-ray diffraction (Figure 1C). Additionally, the crystallite sizes remain similar pre- and post-cation exchange, all averaging approximately 2.9 nm by Scherrer analysis and 3.0 nm by TEM size analysis.

Figure 1A shows the absorption and photoluminescence spectra of the InP/ZnSe, Ag⁺:InP/ZnSe, and Cu⁺:InP/ZnSe QDs. Both doped species of InP show broadened absorption compared to the undoped InP/ZnSe QDs.

Time-resolved photoluminescence measurements show lengthening of the luminescence lifetime from ~30 ns in the undoped QDs to ~270 ns in the Ag⁺-doped QDs and ~360 ns in the Cu⁺ doped QDs (Figure 1B). Upon photoexcitation, the photogenerated hole rapidly localizes to the Cu center within 2 ps,²⁶ reducing the electron–hole wave function overlap, and slowing recombination. While no report has described the photoluminescence of Ag⁺:InP QDs, they appear similar to those of Ag⁺ doped CdSe QDs.

To further understand the behavior of the photoexcited charge carriers in these doped systems, they were examined *in silico* using In₇₇P₇₇ and [In₇₆M₁P₇₇]²⁻ (M = Ag, Cu) model quantum dots. All QDs were terminated by pseudohydrogens (e.g., In₇₇P₇₇H₁₀₈) to provide charge balance and minimize the exaggerated surface effects that may result from small cluster models.

Upon optimization, the geometry of the InP QD around the dopant broke the C_{3v} starting symmetry, as can be seen in Figure 2A. The addition of the metal dopant gives rise to midgap states, which are shown in Figure 2B. To gain insight into the band structure, density of states (DOS) plots are provided in Figure 2C. Examining the DOS for the undoped QD, the valence band can be seen to be comprised primarily of phosphide character, while the conduction band is primarily indium based. Upon doping, the valence and conduction bands are still composed of phosphorus and indium, respectively; however, copper and silver contributions appear in new midgap states. Examining these midgap states shows that, while still primarily composed of phosphorus *p* orbitals, the doping metal contributes *d* orbital character that affects the ionization potential. Between the Cu⁺ and Ag⁺ the highest occupied molecular orbitals (HOMOs) have the same character; however, a reordering of the states between the Cu⁺:InP and Ag⁺:InP can be seen in Figure 2B where the Ag⁺ HOMO–1 is the same as the Cu⁺ HOMO–2 (and *vice versa*). This reordering results in slightly different character for the leaving (hole) orbitals between the Cu⁺:InP and the Ag⁺:InP as can be viewed in Figure 2C. The increased *d* orbital contribution to the midgap states by the Cu⁺ atom with respect to Ag⁺, and different hole character can be ascribed to the difference in *d*-orbital character between the Cu⁺ and Ag⁺ ions. This differing character has been noted previously.¹⁸ Even with this orbital reordering, the excited state properties of both systems are similar. Predicted absorption spectra for these geometries are shown in Figure 2C. Examining the natural transition orbitals (NTOs), inset into the absorption spectra, the first transition is easily determined to be a transition from the occupied midgap state to the unoccupied conduction band.

Due to the similar nature of the transitions between Cu⁺:InP and Ag⁺:InP QDs, a quantitative method is required to differentiate the localization between the two metal dopants. This is achieved using the hole/electron delocalization index (HDI and EDI, respectively) as implemented in Multiwfn.^{27,28} This value is able to give a numerical value for the density over

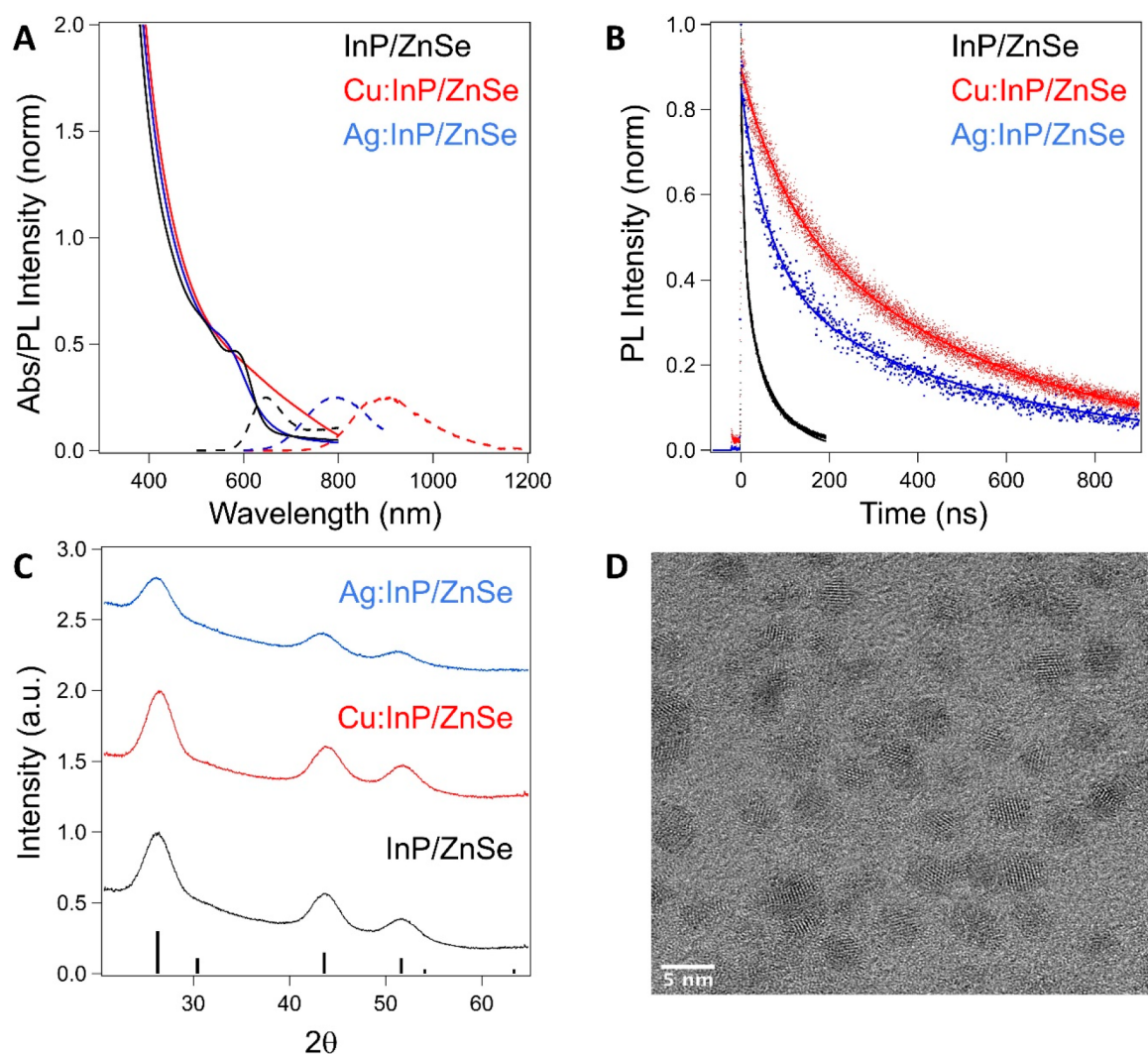


Figure 1. (A) Representative absorption (solid) and photoluminescence (dashed) spectra of InP/ZnSe (black), Ag⁺:InP/ZnSe (blue), and Cu⁺:InP/ZnSe (red) QDs. (B) Time-resolved photoluminescence decay profiles of InP/ZnSe, Ag⁺:InP/ZnSe, and Cu⁺:InP/ZnSe QDs. These data were fit to biexponential functions with the following amplitudes and time constants: InP/ZnSe ($A_1 = 0.466 \pm 0.001$, $\tau_1 = 8.11 \pm 0.04$ ns, $A_2 = 0.393 \pm 0.001$, $\tau_2 = 65.56 \pm 0.16$ ns, $\tau_{\text{weighted}} = 34.4$ ns), Ag⁺:InP/ZnSe ($A_1 = 0.449 \pm 0.004$, $\tau_1 = 64.01 \pm 1.31$ ns, $A_2 = 0.401 \pm 0.003$, $\tau_2 = 517.38 \pm 4.27$ ns, $\tau_{\text{weighted}} = 278.14$ ns), and Cu⁺:InP/ZnSe ($A_1 = 0.264 \pm 0.003$, $\tau_1 = 92.17 \pm 1.74$ ns, $A_2 = 0.631 \pm 0.003$, $\tau_2 = 500.38 \pm 2.35$ ns, $\tau_{\text{weighted}} = 379.8$ ns). (C) Powder XRD patterns of InP/ZnSe, Ag⁺:InP/ZnSe, and Cu⁺:InP/ZnSe QDs. All data were collected at room temperature. (D) Representative TEM image of purified Cu⁺:InP/ZnSe QDs.

the space occupied by the hole/electron corresponding to an excitation. A lower value indicates that the hole or electron is more delocalized in space. Examining Table 1 for the HDI, we found that the most delocalized system (that with the lowest HDI value) is the undoped system. This is expected, as the first transition for the undoped In₇₇P₇₇ QD is a band-to-band type transition. When the dopants are added, the HDI grows, showing the hole localization that we have already observed in Figure 2C, but the HDI for the Cu⁺:InP QDs is greater than that for the Ag⁺:InP QDs. The EDI values for the doped QDs are both similar to that of the undoped QD.

Photoluminescence Quenching with Anthraquinone

To study photoinduced charge transfer from these quantum dots, we examined a series of quinones as electron acceptors. Not only are quinones readily soluble in many of the same organic solvents as quantum dots, but they have previously been shown to accept electrons from photoexcited quantum dots.^{29–32} By an increase in the concentration of anthraqui-

none in the QD solution, a decrease in the QD fluorescence intensity is observed. This decrease can be attributed to the formation of a quantum dot-anthraquinone* adduct, where the electron has been transferred from the photoexcited quantum dot to the anthraquinone adsorbed on the surface. By fitting the loss of luminescence with respect to the concentration of added quencher to the Stern–Volmer equation (eq 1), we can extract a Stern–Volmer quenching constant, K_{SV} , that measures how readily electron transfer occurs between the photoexcited quantum dot and the quinone acceptor. In eq 1, F_0 is defined as the initial photoluminescence intensity, F is defined as the photoluminescence intensity at a given concentration of added quencher, and K_{SV} is defined as the quenching factor or Stern–Volmer constant.

$$\frac{F_0}{F} = 1 + K_{SV}[Q] \quad (1)$$

Figure 3A illustrates that undoped quantum dots retain much of their initial luminescence intensity following addition

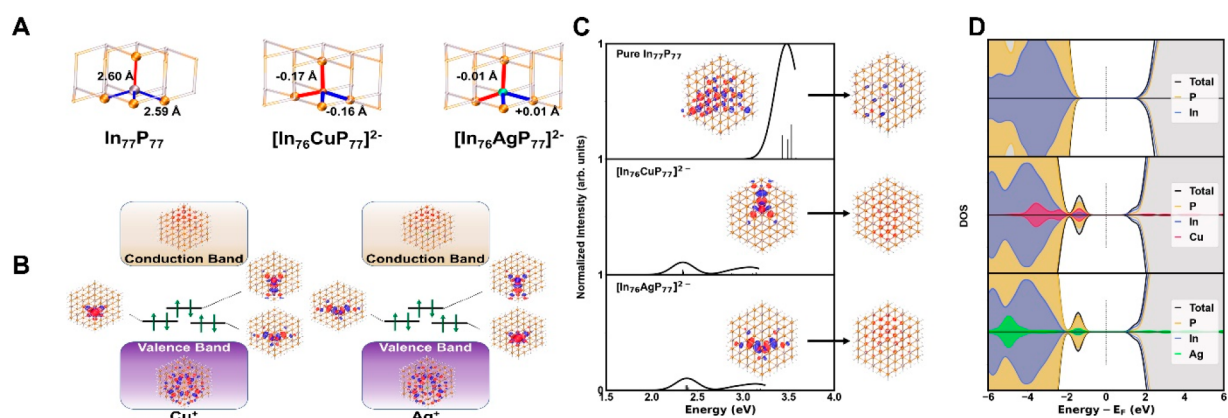


Figure 2. (A) Optimized geometries for the undoped ($\text{In}_{77}\text{P}_{77}$), copper-doped ($[\text{In}_{76}\text{CuP}_{77}]^{2-}$), and silver-doped ($[\text{In}_{76}\text{AgP}_{77}]^{2-}$) quantum dots. The atoms shown are those immediately surrounding the metal center. Changes in the bond length for $[\text{In}_{76}\text{CuP}_{77}]^{2-}$ and $[\text{In}_{76}\text{AgP}_{77}]^{2-}$ are given in relation to the undoped structure. The same color marks a bond that is the same length. (B) Molecular orbital diagrams for the $[\text{In}_{76}\text{CuP}_{77}]^{2-}$ quantum dot (left) and the $[\text{In}_{76}\text{AgP}_{77}]^{2-}$ quantum dot (right). Pictured are the midgap molecular orbitals plotted with an isovalue of 0.01 electron-Bohr⁻³. Black bars mark the midgap states (not drawn to scale), with green arrows marking the occupation for the spin up and spin down electrons. (C) Predicted absorption spectra for the undoped $\text{In}_{77}\text{P}_{77}$ QD, $[\text{In}_{76}\text{CuP}_{77}]^{2-}$, and $[\text{In}_{76}\text{AgP}_{77}]^{2-}$ QDs are shown on the left. Inset into each plot are the natural transition orbitals for the first excitation (numerical values for the energy given in Table 1) with the leaving (hole) orbital on the left and the arriving (electron) orbital on the right. The density of states plots for the undoped QD, the $[\text{In}_{76}\text{CuP}_{77}]^{2-}$ and $[\text{In}_{76}\text{AgP}_{77}]^{2-}$ QDs with positive values corresponding to spin up electrons and negative values corresponding to spin down electrons, are shown on the right.

Table 1. Excitation Energy for the First Transition along with the Corresponding Hole and Electron Delocalized Index for the InP Quantum Dots

dot	excitation [eV] (osc. str.)	hole delocalization index (a.u.)	electron delocalization index (a.u.)
$\text{In}_{77}\text{P}_{77}$	3.429 (0.1854)	2.14	1.22
$[\text{In}_{76}\text{CuP}_{77}]^{2-}$	2.337 (0.0391)	16.89	1.07
$[\text{In}_{76}\text{AgP}_{77}]^{2-}$	2.374 (0.0357)	6.61	1.09

of anthraquinone, indicating low rates of electron transfer relative to PL. However, both the Ag^+ - and Cu^+ -doped samples depicted in Figure 3B and C, respectively, show a marked decrease in their photoluminescence intensity following addition of anthraquinone, with the Cu^+ -doped sample showing the greatest loss of photoluminescence in the series.

Of note in these quenching experiments is the severe negative deviation from the linearity usually expected in simple Stern–Volmer behavior, as shown in Figure 3D–F. This negative deviation has been previously seen during fluorescence quenching of two different conformers of the same fluorophore.^{33,34} A similar negative deviation has been observed in CdS QD/methyl viologen systems.³⁵ In the CdS system two mechanisms of adsorption of methyl viologen were proposed: one in which the acceptor directly associates with the quantum dot surface and one where a weakly bound surface metal ion and/or ligand species dissociates from the surface, followed by adsorption of the acceptor. This dissociation of bound surface ligands followed by adsorption of a new species has also been posited as the mechanism by which InP quantum dots lose under-passivated indium ions at their surfaces to increase photoluminescence quantum yield.³⁶ We hypothesize that a similar process occurs in our InP/ZnSe QDs, in which we see either direct adsorption of anthraquinone to the surface or dissociation of a zinc halide-oleylamine complex, followed by adsorption of the anthraquinone. As we observe that the negative deviation occurs at relatively low concentrations of anthraquinone, we suggest that

the second mechanism, disassociation of a surface cation followed by adsorption of a quinone, dominates the interaction between the quantum dot and the electron acceptor.

To extract a singular K_{SV} from these data, we transform the data of Figure 3D–F using eq 2. In eq 2, F_0 , F , and K_{SV} are defined as in eq 1, and f is defined as the fraction of accessible fluorophore and assumed to be 1.

$$\frac{F_0}{F_0 - F} = \frac{1}{f} + \frac{1}{fK_{\text{SV}}[Q]} \quad (2)$$

After applying this transformation to the PL quenching data, we see that the data can be fit to a single linear equation, as shown in Figure 3G–I. From these fits, we extract K_{SV} values of 2083, 42 700, and 48 558 mol⁻¹·L for InP/ZnSe, Ag^+ :InP/ZnSe, and Cu^+ :InP/ZnSe QDs, respectively, showing an increase in charge transfer by over an order of magnitude for the doped quantum dot-anthraquinone systems. We attribute this enhancement to the extended excited state lifetimes in these doped materials.

Transient Absorption Spectroscopy

To probe the photoinduced charge transfer to anthraquinone further, we turned to transient absorption spectroscopy to examine the bleach kinetics of the photoexcited quantum dots. Transient absorption spectroscopy allows us to examine the decay of the photogenerated conduction-band electron without major convolution from hole dynamics due to the degeneracy of holes at the valence band edge (undoped),³⁷ or deep localization of the holes (doped). Each of the quantum dots showed well-defined bleach features associated with the generation of a conduction band electron (Figure 4A). Furthermore, the kinetics of the bleach recovery are in good agreement with the decay dynamics observed in the time-resolved photoluminescence, as both Ag^+ - and Cu^+ -doped QDs show a longer charge separated state, with the Cu^+ -doped InP/ZnSe QD decay being longer than the Ag^+ -doped InP/ZnSe QD decay (Figure 4B). These results indicate that the photogenerated electrons in the doped QDs live much longer than in the undoped QDs.

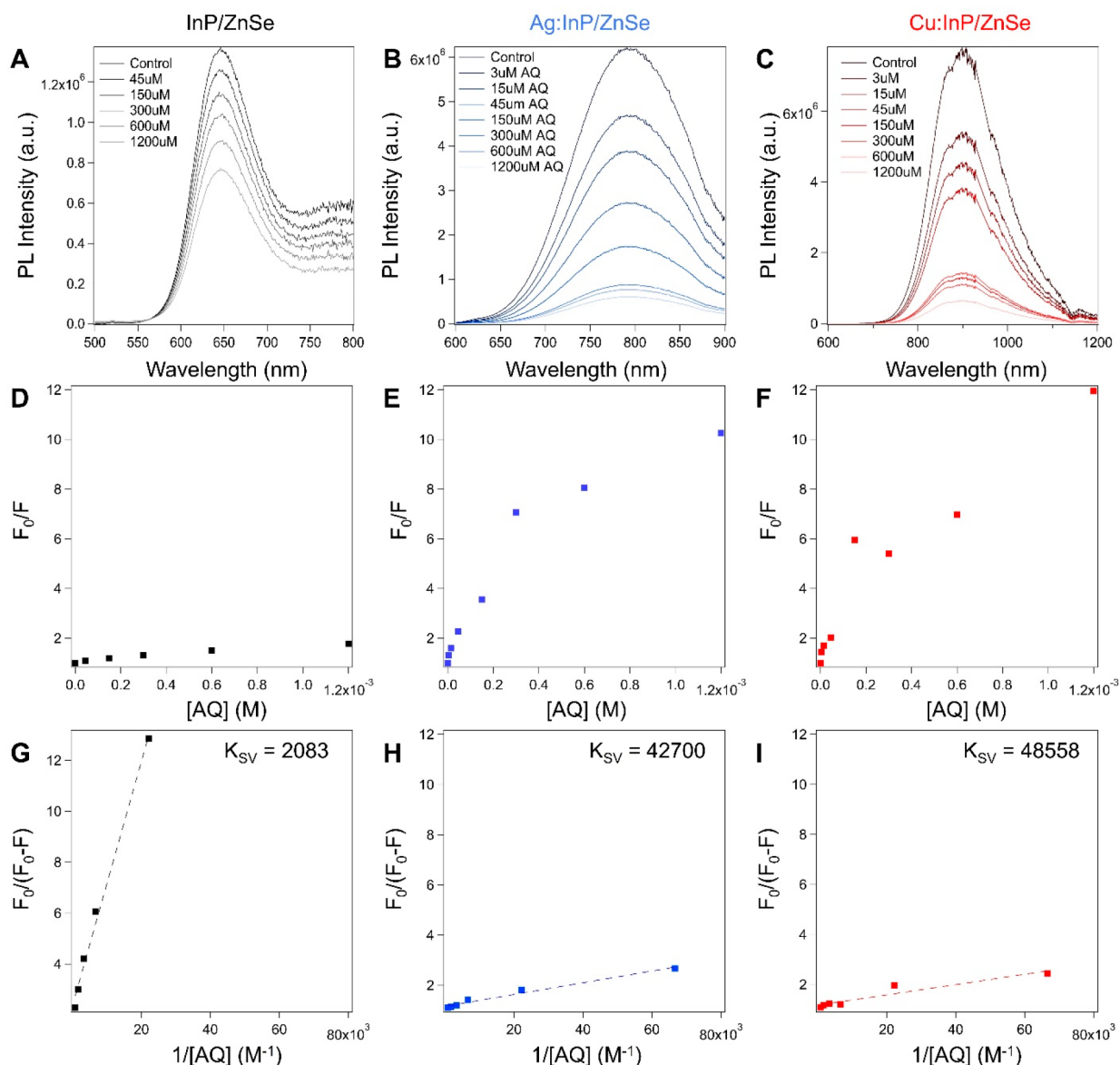


Figure 3. (A) PL quenching of InP/ZnSe QDs upon addition of anthraquinone. (B) PL quenching of Ag⁺:InP/ZnSe QDs upon addition of anthraquinone. (C) PL quenching of Cu⁺:InP/ZnSe QDs upon addition of anthraquinone. (D) Stern–Volmer plot of InP/ZnSe QDs. (E) Stern–Volmer plot of Ag⁺:InP/ZnSe QDs. (F) Stern–Volmer plot of Cu⁺:InP/ZnSe. (G) Transformed Stern–Volmer plot of InP/ZnSe QDs. (H) Transformed Stern–Volmer plot of Ag⁺:InP/ZnSe QDs. (I) Transformed Stern–Volmer plot of Cu⁺:InP/ZnSe QDs.

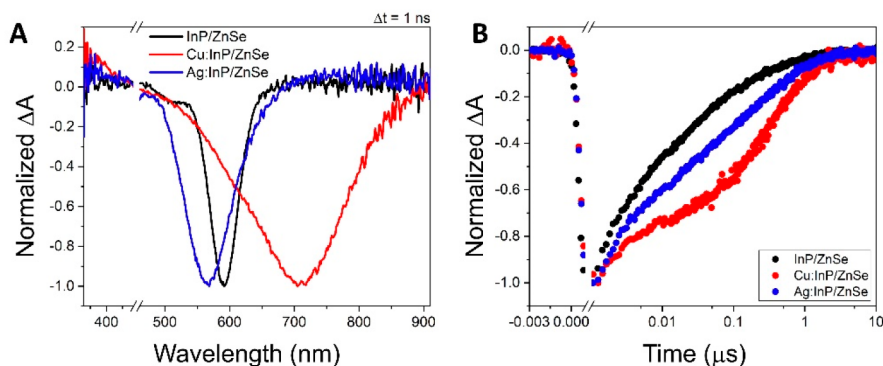


Figure 4. (A) Excitonic bleaches of InP/ZnSe, Ag⁺:InP/ZnSe, and Cu⁺:InP/ZnSe QDs. (B) Bleach-recovery kinetics of respective samples.

By examining the change in bleach recovery kinetics upon addition of anthraquinone, we can determine the relative

amount of electron transfer in doped and undoped quantum dots (Figures S1–S16 and Tables S2–S4). As previously

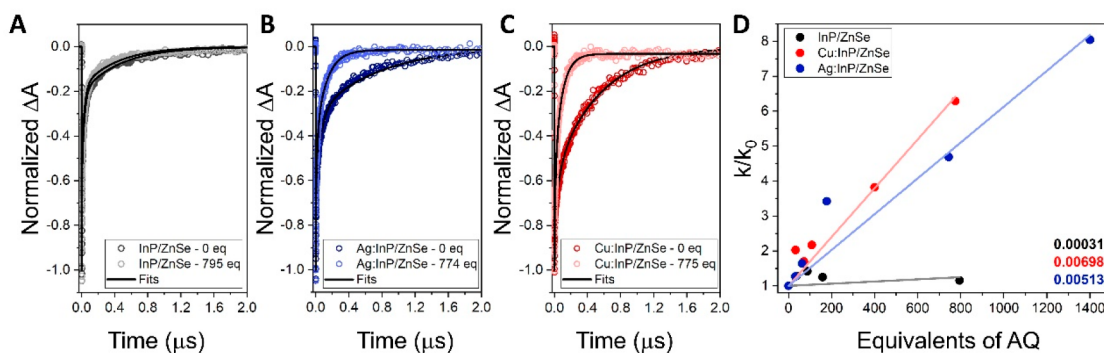


Figure 5. Bleach recovery dynamics of (A) InP/ZnSe, (B) Ag⁺:InP/ZnSe, and (C) Cu⁺:InP/ZnSe QDs with 0 equiv of anthraquinone and ~ 770 equiv of anthraquinone (2.34×10^{-4} M). (D) Comparison of bleach recovery rate constants (k) relative to the original recovery rate constant (k_0). Inset are slopes of each fit.

shown by Zhu et al., electron transfer in quantum dot-anthraquinone systems occurs on the picosecond time scale with recombination to the ground state occurring in a few ns.³⁸ By monitoring the shortening of the excitonic bleach, we are able to determine if the major process occurring is excited-state recombination or charge separation followed by recombination from the quinone. Upon the addition of approximately 770 equiv of anthraquinone to undoped InP/ZnSe QDs, we see that the change in the recovery dynamics is negligible (Figure 5A), indicating that exciton recombination is the preferred pathway for excited state relaxation. In contrast, the Ag⁺- and Cu⁺-doped InP/ZnSe QDs show large changes in the recovery dynamics (Figure 5B and C) upon the addition of the same amount of anthraquinone. Figure 5D compares the three systems and shows that both Ag⁺ and Cu⁺ doped QDs outperform undoped QDs by over an order of magnitude in transferring electrons to the anthraquinone acceptor, in good agreement with the photoluminescence quenching results (Tables S4–S7).

Photoluminescence Quenching Modulated by Acceptor Size

To test the proposed dependence of electron transfer on the surface desorption/acceptor adsorption mechanism described for anthraquinone, we examined PL quenching by electron acceptors of varying sizes, including naphthoquinone and benzoquinone. By using smaller acceptor molecules, the more dominant pathway is expected to shift toward a simple adsorption mechanism, leading to increased PL quenching with all quantum dots. We began these studies by monitoring PL quenching in the quantum dot-benzoquinone system, shown in Figure 6A–C. Not only did we observe much more PL quenching, we also observed greater linearity in the resulting Stern–Volmer plots, Figure 6D–F, suggesting that the mechanism shifts toward a simple adsorption process. From these data, we extract K_{SV} values for InP/ZnSe-benzoquinone, Ag⁺:InP/ZnSe-benzoquinone, and Cu⁺:InP/ZnSe-benzoquinone of 26 744, 28 149, and 62 055 mol⁻¹L, respectively. Notably, upon the addition of higher equivalents of benzoquinone we see the nonlinear deviation begin, suggesting that while the simple adsorption mechanism is most prevalent, the displacement mechanism occurs once all easily available surface sites on the QD are occupied. Additionally, we see negligible changes between losses in the excited state lifetime when comparing doped and undoped quantum dots with adsorbed benzoquinone, indicating both

species are undergoing electron transfer on similar time scales with small acceptors (Figures S17–20, Tables S5–S7).

We next examined PL quenching by naphthoquinone. As it is larger than benzoquinone but smaller than anthraquinone, one would expect the K_{SV} values for these systems to be intermediate to the previously explored quinones, which is what is observed experimentally (Figure 6G–I). All three samples in the series show higher quenching than with anthraquinone but lower than with benzoquinone, with K_{SV} values for undoped, Ag⁺-doped, and Cu⁺-doped InP/ZnSe QDs of 18 991, 27 076, and 44 764 mol⁻¹L, respectively (Figure 6J–L). Interestingly, quantum dot-naphthoquinone systems exhibit nonlinear deviations at higher quencher concentrations than anthraquinone but earlier than benzoquinone, further supporting the interpretation that the size of the acceptor molecule greatly influences the mechanism of adsorption, and hence of electron transfer.

Finally, methyl viologen was investigated, as it is a well-known electron acceptor in QD-molecular systems, showing ultrafast electron transfer.^{39–42} While the size of the methyl viologen is similar to that of anthraquinone, its reduction potential is much larger. Therefore, the study of methyl viologen as an electron acceptor allows determination of whether electron transfer is more impacted by the adsorption mechanism of the acceptor or by driving force. Upon addition of methyl viologen, we once again see remarkable charge transfer enhancement when comparing doped and undoped InP/ZnSe quantum dots (Figure 7A–C). Similar to other acceptors explored here, Ag⁺-doped InP/ZnSe QDs show enhanced electron transfer in comparison to undoped quantum dots but lower charge transfer than Cu⁺-doped InP/ZnSe QDs with K_{SV} values of 12 647, 49 147, and 93 454 mol⁻¹L for InP/ZnSe, Ag⁺:InP/ZnSe, and Cu⁺:InP/ZnSe, respectively (Figure 7D–F). While the K_{SV} values are larger than those for the anthraquinone systems, the overall trend is the same, with Cu⁺-doped QDs showing almost an order of magnitude enhancement in electron transfer. We therefore attribute the increased K_{SV} values to the higher driving force for electron transfer to methyl viologen than anthraquinone. By examining a comparison of reduction potential vs K_{SV} we see that the larger acceptors show over an order of magnitude increase between the undoped and doped species when compared to a sample with similar reduction potential (Figures S21 and S22). Additionally, we see that Cu⁺-doped species outperform Ag⁺-doped species in all cases, which we attribute to the more highly localized hole at the band edges, and thus,

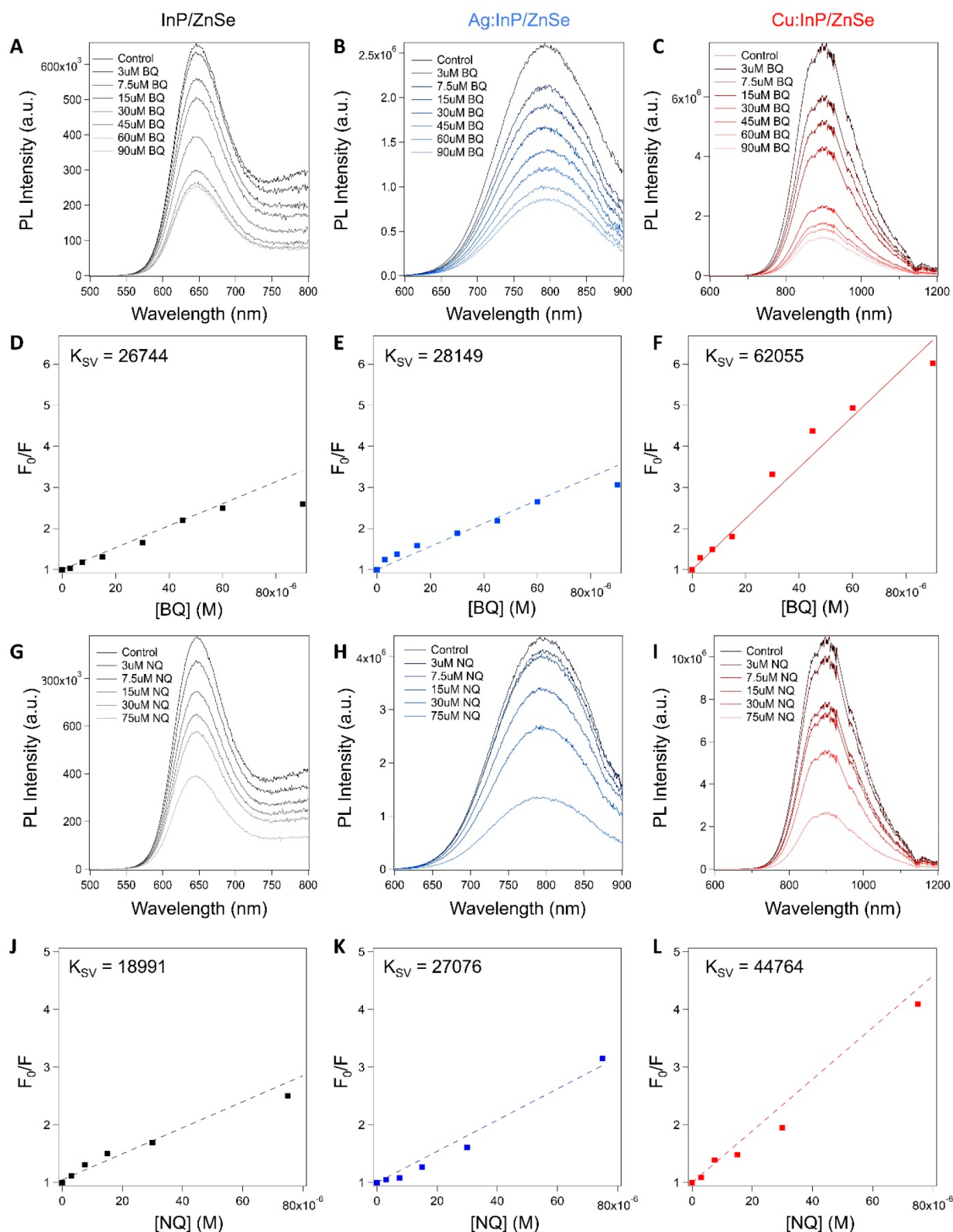


Figure 6. (A) PL quenching of InP/ZnSe QDs with addition of benzoquinone. (B) PL quenching of Ag⁺:InP/ZnSe QDs with addition of benzoquinone. (C) PL quenching of Cu⁺:InP/ZnSe QDs with addition of benzoquinone. (D) Stern–Volmer plot of InP/ZnSe QDs with benzoquinone. (E) Stern–Volmer plot of Ag⁺:InP/ZnSe QDs with benzoquinone. (F) Stern–Volmer plot of Cu⁺:InP/ZnSe QDs with benzoquinone. (G) PL quenching of InP/ZnSe QDs with the addition of naphthoquinone. (H) PL quenching of Ag⁺:InP/ZnSe QDs with the addition of naphthoquinone. (I) PL quenching of Cu⁺:InP/ZnSe QDs with addition of naphthoquinone. (J) Stern–Volmer plot of InP/ZnSe QDs with naphthoquinone. (K) Stern–Volmer plot of Ag⁺:InP/ZnSe QDs with naphthoquinone. (L) Stern–Volmer plot of Cu⁺:InP/ZnSe QDs with naphthoquinone.

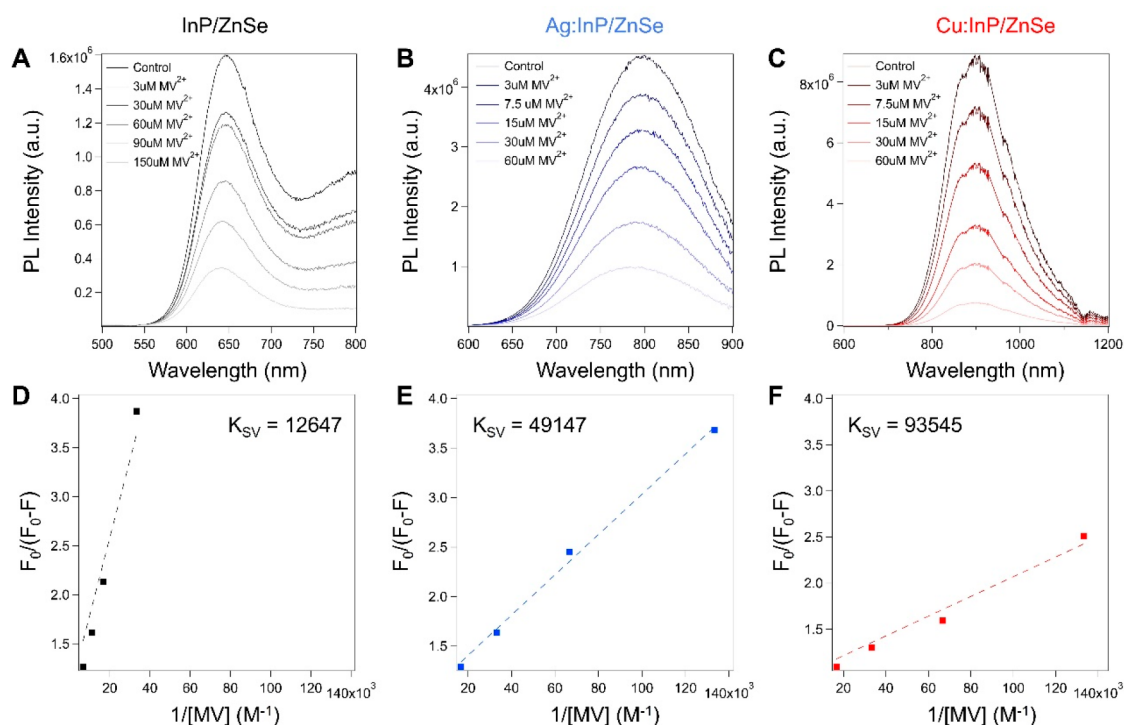


Figure 7. Photoluminescence quenching of (A) InP/ZnSe QDs, (B) Ag⁺:InP/ZnSe QDs, and (C) Cu⁺:InP/ZnSe QDs in the presence of methyl viologen. (D) Transformed Stern–Volmer plot of InP/ZnSe QDs. (E) Transformed Stern–Volmer plot of Ag⁺:InP/ZnSe QDs. (F) Transformed Stern–Volmer plot of Cu⁺:InP/ZnSe QDs.

the reducing potential of both species is nearly identical (Figure S23).

CONCLUSION

In this work, we have found that coinage-metal-doped InP quantum dots show remarkably enhanced electron transfer to a wide variety of electron acceptors compared to undoped InP/ZnSe quantum dots. Through *ab initio* DFT calculations, we confirm the assignment of hole localization to the dopant, with increased structural distortion and elevated hole and electron localization for Cu⁺- versus Ag⁺-doped QDs. Analysis of photoluminescence quenching shows that electron transfer is enhanced by over an order of magnitude when the quantum dot is paired with a bulky acceptor such as anthraquinone. By changing the size of our electron acceptors, we are able to preferentially choose the dominant adsorption pathway of the electron acceptor as either direct adsorption or ligand dissociation, followed by adsorption. With acceptors that require ligand dissociation, the long-lived excited state lifetimes generated by dopants were found to be necessary for efficient electron transfer, and larger differences between doped and undoped quantum dots are observed. However, when small acceptors were added, the difference in the electron transfer between doped and undoped quantum dots is smaller. Transient absorption spectroscopy was performed to examine the electron dynamics in these systems, showing greatly enhanced lifetimes of photogenerated conduction band electrons in the doped QDs, consistent with the formation of an emissive charge transfer excited state. This work provides new insight into the role of dopant-induced wave function localization on charge transfer from quantum dot photosensitizers, paving the way for improved design and implementation of these materials as photoredox catalysts.

EXPERIMENTAL METHODS

Methods and Materials

All glassware was dried in a 160 °C oven overnight prior to use. All reactions were run under an inert atmosphere of nitrogen using a glovebox or standard Schlenk techniques. Zinc chloride (>98%), tris-diethylaminophosphine (97%), copper(II) chloride (≥98%), indium(III) chloride (97%), silver(I) chloride (99%), and anhydrous ethanol were purchased from Millipore-Sigma, stored in a nitrogen glovebox or desiccator, and used without further purification. Anthraquinone, benzoquinone, naphthoquinone, and methyl viologen dchloride were purchased from Millipore-Sigma and stored in an inert atmosphere glovebox. Methyl viologen diiodide was formed via salt metathesis from methyl viologen dichloride.⁴³

Oleylamine and toluene, which were purchased from Millipore-Sigma, were dried over CaH₂, distilled, and stored over 4 Å sieves in a nitrogen glovebox. Omni Trace nitric acid was purchased from EMD Millipore and used without purification. Water, 18.2 MΩ, was collected from an EMD Millipore water purification system.

Synthesis of InP/ZnSe, Ag⁺:InP/ZnSe, and Cu⁺:InP/ZnSe Quantum Dots

0.23 mmol portion of an indium halide, 1.1 mmol of ZnCl₂, and 2.5 mL of dried and distilled oleylamine were added to a 15 mL 3-neck flask. The solution was then placed under vacuum at 120 °C and degassed for 1 h. The vessel was then placed under an inert atmosphere and heated to 180 °C. Once the reaction temperature was reached, 0.23 mL of tris-diethylaminophosphine (0.8 mmol) was rapidly injected. The reaction was allowed to proceed for 20 min, after which 0.5 mL of previously prepared 1 M TOP-Se was slowly injected. At 60 min, the temperature was increased to 200 °C and held there for an additional 60 min. The flask was then cooled down to room temperature before being moved into a nitrogen glovebox for purification. The nanocrystals were precipitated with anhydrous ethanol, centrifuged at 7830 rpm, and suspended in toluene. This procedure was repeated 5 times before any additional sample analysis was performed.

Doped samples were synthesized following the same method as above. However, 120 min after TOP=Se addition, the temperature was decreased to 150 °C. Once this temperature was reached, the copper halide (CuCl₂) or silver halide (AgCl) solution was slowly injected (1 mL at 2 mL/h). After the injection had completed, the temperature was increased to 210 °C and held there for 1.5 h. Purification procedures remained the same as those for the undoped samples.

Characterization

UV–vis absorption spectroscopy was carried out using an Agilent Cary 5000 spectrophotometer. Photoluminescence spectroscopy was performed using an Edinburgh FLS 1000 Fluorimeter located in the University of Washington's MEM-C shared user facility. Concentrations of QD solutions were set to 300 nM via dilution as determined using the method developed in ref 10.

For quenching experiments, samples were cycled into an inert atmosphere glovebox, and microliter volumes of toluene solutions containing the electron acceptor were added to avoid convolution from large dilution effects (the concentration of the added solution of electron acceptor was 10 mM (from the range of 3 μM to 45 μM) or 100 mM (more than 45 μM acceptor added). The total added volume of solvent in any sample did not exceed 100 μL. Excitation for quantum dot/antraquinone systems occurred at 450 nm to avoid coexcitation. Quantum dot/benzoquinone, quantum dot/naphthoquinone, and quantum dot/methyl viologen systems were all excited at 402 nm.

Preparation of the QD-MV²⁺ system varied from other quenching experiment preparations due to the insolubility of MV²⁺ in common organic solvents. Instead, methyl viologen diiodide was suspended in dry methanol and sonicated before being brought back into an inert atmosphere glovebox and added to the quantum dot solution.⁴⁴

Powder X-ray diffraction data were recorded on a Bruker D8 Discover instrument with the IμS 2-D XRD system at the University of Washington's Molecular Analysis Facility. TEM images were obtained on an FEI Technai G2 F20 microscope at the University of Washington's Molecular Analysis Facility. TEM samples were prepared by spotting 5 μL of a dilute solution of QDs dispersed in toluene onto an ultrathin carbon on a holey carbon support film purchased from Ted Pella. A PerkinElmer Optima 8300 inductively coupled plasma–optical emission spectrophotometer was used for elemental analysis.

Computational Methods

Quasi-spherical InP quantum dots, In₇₇P₇₇ (diameter ~2 nm), were constructed using the bulk Zinc Blende crystal structure. The undoped structure conformed to C_{3v} symmetry before optimization. Doped structures were built from the InP core by replacing one In center with a dopant atom to form In₇₆MP₇₇ (M = Cu⁺, Ag⁺). Ground-state geometric optimizations were performed, and the structures were considered optimized when both the forces [maximum and root-mean-square (rms) of the force 0.000450 and 0.000300 hartree/Bohr, respectively] and displacement [maximum and rms displacement 0.00018 and 0.0012 Bohr, respectively] values were below the threshold criteria. Surface dangling bonds were terminated using a pseudohydrogen capping scheme to compensate surface ions (±1/3 to passivate the In/P ions, respectively) resulting in an In₇₇P₇₇H₁₀₈ structure for the pure, nondoped system. In order to maintain a proper charge on the M⁺ ion, the doped systems have an overall charge of (–2). Similar methods have been used in previous studies on doped semiconductor nanocrystals.^{18,45–47} These systems are expected to exhibit quantum confinement (Bohr exciton radius is 10 nm for InP⁴⁸); however, the diameters of the prepared dots are similar to those able to be created experimentally.⁴⁹ Calculations were conducted using the Gaussian software package⁵⁰ using the Perdew, Burke, and Ernzerhof hybrid functional (PBE0)^{51–53} to compute the Kohn–Sham ground-state electronic structure. The Los Alamos National Lab 2-Double Zeta (LANL2DZ) pseudopotential and associated basis sets was used.^{54–57} This combination is able to fairly accurately reproduce the experimentally observed 3.7 eV band gap (computational gap is 3.89 eV, + 5% in relation to experiment).^{47,49}

The electronic structures of excited states were calculated using time-dependent DFT (TD-DFT) within the linear-response framework.^{58–60}

Transient Absorption Measurements

Transient absorption measurements were performed using an EOS unit from Ultrafast Systems at the University of Washington's Molecular Analysis Facility. The pump wavelength of 450 nm was chosen to avoid coexcitation of the quinone acceptor. It was generated via a Coherent Inc./Light Source OPerA optical parametric amplifier, with a power of 400 μW measured through a 200 μm pinhole. The probe white light was generated by using an external Q-switched Nd:YAG laser with an electronic delay. The collinear pump and probe beams overlapped with the sample.

■ ASSOCIATED CONTENT

Supporting Information

The Supporting Information is available free of charge at <https://pubs.acs.org/doi/10.1021/acsnanoscienceau.3c00029>.

Transient absorption spectra; time-resolved photoluminescence quenching experiments with benzoquinone; additional SV plots; and tables containing time constants for photoluminescence and transient absorption bleach decays (PDF)

■ AUTHOR INFORMATION

Corresponding Author

Brandi M. Cossairt – Department of Chemistry, University of Washington, Seattle, Washington 98195-1700, United States; orcid.org/0000-0002-9891-3259; Email: cossairt@uw.edu

Authors

Forrest W. Eagle – Department of Chemistry, University of Washington, Seattle, Washington 98195-1700, United States
Samantha Harvey – Department of Chemistry, University of Washington, Seattle, Washington 98195-1700, United States
Ryan Beck – Department of Chemistry, University of Washington, Seattle, Washington 98195-1700, United States; orcid.org/0000-0002-2953-970X
Xiaosong Li – Department of Chemistry, University of Washington, Seattle, Washington 98195-1700, United States; orcid.org/0000-0001-7341-6240
Daniel R. Gamelin – Department of Chemistry, University of Washington, Seattle, Washington 98195-1700, United States; orcid.org/0000-0003-2888-9916

Complete contact information is available at: <https://pubs.acs.org/doi/10.1021/acsnanoscienceau.3c00029>

Author Contributions

CRediT: **Forrest W. Eagle** conceptualization, data curation, formal analysis, investigation, methodology, writing-original draft; **Samantha Harvey** formal analysis, investigation; **Ryan A. Beck** formal analysis, investigation, methodology, visualization, writing-original draft; **Xiaosong Li** resources, software, supervision; **Daniel R. Gamelin** resources, funding acquisition, supervision, validation, writing-review & editing; **Brandi M. Cossairt** conceptualization, data curation, funding acquisition, methodology, project administration, resources, supervision, validation, writing-review & editing.

Notes

The authors declare no competing financial interest.

ACKNOWLEDGMENTS

This research was supported by the U.S. National Science Foundation (NSF) through the UW Molecular Engineering Materials Center (MEM-C), a Materials Research Science and Engineering Center (Grant Nos. DMR-1719797 and DMR-2308979). The authors acknowledge the use of facilities and instrumentation supported by the U.S. National Science Foundation through the UW MEM-C (DMR-1719797 and DMR-2308979). Part of this work was conducted at the Molecular Analysis Facility, a National Nanotechnology Coordinated Infrastructure site at the University of Washington, which is supported, in part, by the National Science Foundation (Grant No. NNCI-1542101), the University of Washington, the Molecular Engineering and Sciences Institute, and the Clean Energy Institute. The computational work was facilitated through the use of advanced computational, storage, and networking infrastructure provided by the Hyak super-computer system and funded by the STF at the University of Washington. S.H. gratefully acknowledges fellowship support from the Department of Energy Office of Basic Sciences (Grant No. DE-SC0021232).

REFERENCES

- (1) Nakajima, T.; Tamaki, Y.; Ueno, K.; Kato, E.; Nishikawa, T.; Ohkubo, K.; Yamazaki, Y.; Morimoto, T.; Ishitani, O. Photocatalytic Reduction of Low Concentration of CO₂. *J. Am. Chem. Soc.* **2016**, *138* (42), 13818–13821.
- (2) Sahara, G.; Kumagai, H.; Maeda, K.; Kaeffer, N.; Artero, V.; Higashi, M.; Abe, R.; Ishitani, O. Photoelectrochemical Reduction of CO₂ Coupled to Water Oxidation Using a Photocathode with a Ru(II)-Re(I) Complex Photocatalyst and a CoO_x/TaON Photoanode. *J. Am. Chem. Soc.* **2016**, *138* (42), 14152–14158.
- (3) Brus, L. Electronic Wave Functions in Semiconductor Clusters: Experiment and Theory. *J. Phys. Chem.* **1986**, *90* (12), 2555–2560.
- (4) Toufanian, R.; Chern, M.; Kong, V. H.; Dennis, A. M. Engineering Brightness-Matched Indium Phosphide Quantum Dots. *Chem. Mater.* **2021**, *33* (6), 1964–1975.
- (5) Peng, X.; Schlamp, M. C.; Kadavanich, A. V.; Alivisatos, A. P. Epitaxial Growth of Highly Luminescent CdSe/CdS Core/Shell Nanocrystals with Photostability and Electronic Accessibility. *J. Am. Chem. Soc.* **1997**, *119* (30), 7019–7029.
- (6) Lim, J.; Bae, W. K.; Lee, D.; Nam, M. K.; Jung, J.; Lee, C.; Char, K.; Lee, S. InP@ZnSeS, Core@Composition Gradient Shell Quantum Dots with Enhanced Stability. *Chem. Mater.* **2011**, *23* (20), 4459–4463.
- (7) Murcia, M. J.; Shaw, D. L.; Woodruff, H.; Naumann, C. A.; Young, B. A.; Long, E. C. Facile Sonochemical Synthesis of Highly Luminescent ZnS-Shelled CdSe Quantum Dots. *Chem. Mater.* **2006**, *18* (9), 2219–2225.
- (8) Hughes, K. E.; Stein, J. L.; Friedfeld, M. R.; Cossairt, B. M.; Gamelin, D. R. Effects of Surface Chemistry on the Photophysics of Colloidal InP Nanocrystals. *ACS Nano* **2019**, *13* (12), 14198–14207.
- (9) Kirkwood, N.; Monchen, J. O. V.; Crisp, R. W.; Grimaldi, G.; Bergstein, H. A. C.; du Fossé, I.; van der Stam, W.; Infante, I.; Houtepen, A. J. Finding and Fixing Traps in II-VI and III-V Colloidal Quantum Dots: The Importance of Z-Type Ligand Passivation. *J. Am. Chem. Soc.* **2018**, *140* (46), 15712–15723.
- (10) Reiss, P.; Protière, M.; Li, L. Core/Shell Semiconductor Nanocrystals. *Small* **2009**, *5* (2), 154–168.
- (11) Mičić, O. I.; Sprague, J.; Lu, Z.; Nozik, A. J. Highly Efficient Band-edge Emission from InP Quantum Dots. *Appl. Phys. Lett.* **1996**, *68* (22), 3150–3152.
- (12) Jones, M.; Nedeljkovic, J.; Ellingson, R. J.; Nozik, A. J.; Rumbles, G. Photoenhancement of Luminescence in Colloidal CdSe Quantum Dot Solutions. *J. Phys. Chem. B* **2003**, *107* (41), 11346–11352.
- (13) Jiang, Y.; Wang, C.; Rogers, C. R.; Kodaimati, M. S.; Weiss, E. A. Regio- and Diastereoselective Intermolecular [2 + 2] Cycloadditions Photocatalysed by Quantum Dots. *Nat. Chem.* **2019**, *11* (11), 1034–1040.
- (14) Jones, L. O.; Mosquera, M. A.; Jiang, Y.; Weiss, E. A.; Schatz, G. C.; Ratner, M. A. Thermodynamics and Mechanism of a Photocatalyzed Stereoselective [2 + 2] Cycloaddition on a CdSe Quantum Dot. *J. Am. Chem. Soc.* **2020**, *142* (36), 15488–15495.
- (15) Yu, S.; Fan, X.-B.; Wang, X.; Li, J.; Zhang, Q.; Xia, A.; Wei, S.; Wu, L.-Z.; Zhou, Y.; Patzke, G. R. Efficient Photocatalytic Hydrogen Evolution with Ligand Engineered All-Inorganic InP and InP/ZnS Colloidal Quantum Dots. *Nature Commun.* **2018**, *9* (1), 4009.
- (16) Han, Z.; Qiu, F.; Eisenberg, R.; Holland, P. L.; Krauss, T. D. Robust Photogeneration of H₂ in Water Using Semiconductor Nanocrystals and a Nickel Catalyst. *Science* **2012**, *338* (6112), 1321–1324.
- (17) Knowles, K. E.; Nelson, H. D.; Kilburn, T. B.; Gamelin, D. R. Singlet-Triplet Splittings in the Luminescent Excited States of Colloidal Cu⁺:CdSe, Cu⁺:InP, and CuInS₂ Nanocrystals: Charge-Transfer Configurations and Self-Trapped Excitons. *J. Am. Chem. Soc.* **2015**, *137* (40), 13138–13147.
- (18) Nelson, H. D.; Hinterding, S. O. M.; Fainblat, R.; Creutz, S. E.; Li, X.; Gamelin, D. R. Mid-Gap States and Normal vs Inverted Bonding in Luminescent Cu⁺- and Ag⁺-Doped CdSe Nanocrystals. *J. Am. Chem. Soc.* **2017**, *139* (18), 6411–6421.
- (19) Nelson, H. D.; Li, X.; Gamelin, D. R. Computational Studies of the Electronic Structures of Copper-Doped CdSe Nanocrystals: Oxidation States, Jahn-Teller Distortions, Vibronic Bandshapes, and Singlet-Triplet Splittings. *J. Phys. Chem. C* **2016**, *120* (10), 5714–5723.
- (20) Whitham, P. J.; Knowles, K. E.; Reid, P. J.; Gamelin, D. R. Photoluminescence Blinking and Reversible Electron Trapping in Copper-Doped CdSe Nanocrystals. *Nano Lett.* **2015**, *15* (6), 4045–4051.
- (21) Knowles, K. E.; Hartstein, K. H.; Kilburn, T. B.; Marchioro, A.; Nelson, H. D.; Whitham, P. J.; Gamelin, D. R. Luminescent Colloidal Semiconductor Nanocrystals Containing Copper: Synthesis, Photophysics, and Applications. *Chem. Rev.* **2016**, *116* (18), 10820–10851.
- (22) Grandhi, G. K.; Tomar, R.; Viswanatha, R. Study of Surface and Bulk Electronic Structure of II-VI Semiconductor Nanocrystals Using Cu as a Nanosensor. *ACS Nano* **2012**, *6* (11), 9751–9763.
- (23) Mundy, M. E.; Eagle, F. W.; Hughes, K. E.; Gamelin, D. R.; Cossairt, B. M. Synthesis and Spectroscopy of Emissive, Surface-Modified, Copper-Doped Indium Phosphide Nanocrystals. *ACS Materials Lett.* **2020**, *2* (6), 576–581.
- (24) Hughes, K. E.; Hartstein, K. H.; Gamelin, D. R. Photodoping and Transient Spectroscopies of Copper-Doped CdSe/CdS Nanocrystals. *ACS Nano* **2018**, *12* (1), 718–728.
- (25) Hassan, A.; Zhang, X.; Liu, C.; Snee, P. T. Electronic Structure and Dynamics of Copper-Doped Indium Phosphide Nanocrystals Studied with Time-Resolved X-Ray Absorption and Large-Scale DFT Calculations. *J. Phys. Chem. C* **2018**, *122* (20), 11145–11151.
- (26) Prins, P. T.; Spruijt, D. A. W.; Mangnus, M. J. J.; Rabouw, F. T.; Vanmaekelbergh, D.; de Mello Donega, C.; Geiregat, P. Slow Hole Localization and Fast Electron Cooling in Cu-Doped InP/ZnSe Quantum Dots. *J. Phys. Chem. Lett.* **2022**, *13* (42), 9950–9956.
- (27) Lu, T.; Chen, F. Multiwfn: A Multifunctional Wavefunction Analyzer. *J. Comput. Chem.* **2012**, *33* (5), 580–592.
- (28) Liu, Z.; Lu, T.; Chen, Q. An Sp-Hybridized All-Carboatomic Ring, Cyclo[18]Carbon: Electronic Structure, Electronic Spectrum, and Optical Nonlinearity. *Carbon* **2020**, *165*, 461–467.
- (29) Aruda, K. O.; Bohlmann Kunz, M.; Tagliazucchi, M.; Weiss, E. A. Temperature-Dependent Permeability of the Ligand Shell of PbS Quantum Dots Probed by Electron Transfer to Benzoquinone. *J. Phys. Chem. Lett.* **2015**, *6* (14), 2841–2846.
- (30) Long, D.; Wu, G.; Wang, W.; Yao, S. Photo-Induced Interfacial Electron Transfer from CdSe Quantum Dots to Surface-Bound p-Benzoquinone and Anthraquinone. *Res. Chem. Intermed.* **2007**, *33* (7), 655–661.

- (31) Knowles, K. E.; Malicki, M.; Weiss, E. A. Dual-Time Scale Photoinduced Electron Transfer from PbS Quantum Dots to a Molecular Acceptor. *J. Am. Chem. Soc.* **2012**, *134* (30), 12470–12473.
- (32) Lou, Y.; Chen, X.; Samia, A. C.; Burda, C. Femtosecond Spectroscopic Investigation of the Carrier Lifetimes in Digenite Quantum Dots and Discrimination of the Electron and Hole Dynamics via Ultrafast Interfacial Electron Transfer. *J. Phys. Chem. B* **2003**, *107* (45), 12431–12437.
- (33) Htun, T. A Negative Deviation from Stern-Volmer Equation in Fluorescence Quenching. *J. Fluoresc.* **2004**, *14* (2), 217–222.
- (34) Boaz, H.; Rollefson, G. K. The Quenching of Fluorescence. Deviations from the Stern-Volmer Law. *J. Am. Chem. Soc.* **1950**, *72* (8), 3435–3443.
- (35) Peterson, M. D.; Jensen, S. C.; Weinberg, D. J.; Weiss, E. A. Mechanisms for Adsorption of Methyl Viologen on CdS Quantum Dots. *ACS Nano* **2014**, *8* (3), 2826–2837.
- (36) Calvin, J. J.; Swabeck, J. K.; Sedlak, A. B.; Kim, Y.; Jang, E.; Alivisatos, A. P. Thermodynamic Investigation of Increased Luminescence in Indium Phosphide Quantum Dots by Treatment with Metal Halide Salts. *J. Am. Chem. Soc.* **2020**, *142* (44), 18897–18906.
- (37) Klimov, V. I. Optical Nonlinearities and Ultrafast Carrier Dynamics in Semiconductor Nanocrystals. *J. Phys. Chem. B* **2000**, *104* (26), 6112–6123.
- (38) Zhu, H.; Song, N.; Lian, T. Controlling Charge Separation and Recombination Rates in CdSe/ZnS Type I Core-Shell Quantum Dots by Shell Thicknesses. *J. Am. Chem. Soc.* **2010**, *132* (42), 15038–15045.
- (39) Morris-Cohen, A. J.; Peterson, M. D.; Frederick, M. T.; Kamm, J. M.; Weiss, E. A. Evidence for a Through-Space Pathway for Electron Transfer from Quantum Dots to Carboxylate-Functionalized Viologens. *J. Phys. Chem. Lett.* **2012**, *3* (19), 2840–2844.
- (40) Wang, Y.-F.; Wang, H.-Y.; Li, Z.-S.; Zhao, J.; Wang, L.; Chen, Q.-D.; Wang, W.-Q.; Sun, H.-B. Electron Extraction Dynamics in CdSe and CdSe/CdS/ZnS Quantum Dots Adsorbed with Methyl Viologen. *J. Phys. Chem. C* **2014**, *118* (31), 17240–17246.
- (41) Zhao, F.; Li, Q.; Han, K.; Lian, T. Mechanism of Efficient Viologen Radical Generation by Ultrafast Electron Transfer from CdS Quantum Dots. *J. Phys. Chem. C* **2018**, *122* (30), 17136–17142.
- (42) Wu, K.; Song, N.; Liu, Z.; Zhu, H.; Rodríguez-Córdoba, W.; Lian, T. Interfacial Charge Separation and Recombination in InP and Quasi-Type II InP/CdS Core/Shell Quantum Dot-Molecular Acceptor Complexes. *J. Phys. Chem. A* **2013**, *117* (32), 7561–7570.
- (43) Macfarlane, A. J.; Williams, R. J. P. Charge-Transfer Properties of Some Paraquat Salts. *J. Chem. Soc., A* **1969**, 1517.
- (44) Matylitsky, V. V.; Dworak, L.; Breus, V. V.; Basché, T.; Wachtveitl, J. Ultrafast Charge Separation in Multiexcited CdSe Quantum Dots Mediated by Adsorbed Electron Acceptors. *J. Am. Chem. Soc.* **2009**, *131* (7), 2424–2425.
- (45) Goings, J. J.; Schimpf, A. M.; May, J. W.; Johns, R. W.; Gamelin, D. R.; Li, X. Theoretical Characterization of Conduction-Band Electrons in Photodoped and Aluminum-Doped Zinc Oxide (AZO) Quantum Dots. *J. Phys. Chem. C* **2014**, *118* (46), 26584–26590.
- (46) Petrone, A.; Beck, R. A.; Kasper, J. M.; Li, X.; Huang, Y.; Crane, M.; Pauzauskie, P. Electronic Structures and Spectroscopic Signatures of Silicon-Vacancy Containing Nanodiamonds. *Phys. Rev. B* **2018**, *98* (20), 205405.
- (47) Park, N.; Eagle, F. W.; DeLarme, A. J.; Monahan, M.; LoCurto, T.; Beck, R.; Li, X.; Cossairt, B. M. Tuning the Interfacial Stoichiometry of InP Core and InP/ZnSe Core/Shell Quantum Dots. *J. Chem. Phys.* **2021**, *155* (8), 084701.
- (48) Chen, B.; Li, D.; Wang, F. InP Quantum Dots: Synthesis and Lighting Applications. *Small* **2020**, *16* (32), 2002454.
- (49) Cho, E.; Kim, T.; Choi, S.; Jang, H.; Min, K.; Jang, E. Optical Characteristics of the Surface Defects in InP Colloidal Quantum Dots for Highly Efficient Light-Emitting Applications. *ACS Appl. Nano Mater.* **2018**, *1* (12), 7106–7114.
- (50) Frisch, M. J.; Trucks, G. W.; Schlegel, H. B.; Scuseria, G. E.; Robb, M. A.; Cheeseman, J. R.; Scalmani, G.; Barone, V.; Mennucci, B.; Petersson, G. A.; Nakatsuji, H.; Caricato, M.; Li, X.; Hratchian, H. P.; Izmaylov, A. F.; Bloino, J.; Zheng, G.; Sonnenberg, J. L.; Hada, M.; Ehara, M.; Toyota, K.; Fukuda, R.; Hasegawa, J.; Ishida, M.; Nakajima, T.; Honda, Y.; Kitao, O.; Nakai, H.; Vreven, T.; Montgomery, J. A., Jr.; Peralta, P. E.; Ogliaro, F.; Bearpark, M.; Heyd, J. J.; Brothers, E.; Kudin, K. N.; Staroverov, V. N.; Kobayashi, R.; Normand, J.; Raghavachari, K.; Rendell, A.; Burant, J. C.; Iyengar, S. S.; Tomasi, J.; Cossi, M.; Rega, N.; Millam, N. J.; Klene, M.; Knox, J. E.; Cross, J. B.; Bakken, V.; Adamo, C.; Jaramillo, J.; Gomperts, R.; Stratmann, R. E.; Yazyev, O.; Austin, A. J.; Cammi, R.; Pomelli, C.; Ochterski, J. W.; Martin, R. L.; Morokuma, K.; Zakrzewski, V. G.; Voth, G. A.; Salvador, P.; Dannenberg, J. J.; Dapprich, S.; Daniels, A. D.; Farkas, Ö.; Ortiz, J. V.; Cioslowski, J.; Fox, D. J. *Gaussian 16*, revision B.01; Gaussian, Inc., 2016.
- (51) Ernzerhof, M.; Scuseria, G. E. Assessment of the Perdew-Burke-Ernzerhof Exchange-Correlation Functional. *J. Chem. Phys.* **1999**, *110* (11), 5029–5036.
- (52) Adamo, C.; Barone, V. Toward Reliable Density Functional Methods without Adjustable Parameters: The PBE0 Model. *J. Chem. Phys.* **1999**, *110* (13), 6158–6170.
- (53) Perdew, J. P.; Burke, K.; Ernzerhof, M. Generalized Gradient Approximation Made Simple. *Phys. Rev. Lett.* **1997**, *78* (7), 1396–1396.
- (54) Dunning, T. H.; Hay, P. J. *Modern Theoretical Chemistry*; Plenum: New York, 1977; Vol. 3, pp 1–28.
- (55) Hay, P. J.; Wadt, W. R. Ab Initio Effective Core Potentials for Molecular Calculations. Potentials for the Transition Metal Atoms Sc to Hg. *J. Chem. Phys.* **1985**, *82* (1), 270–283.
- (56) Wadt, W. R.; Hay, P. J. Ab Initio Effective Core Potentials for Molecular Calculations. Potentials for Main Group Elements Na to Bi. *J. Chem. Phys.* **1985**, *82* (1), 284–298.
- (57) Hay, P. J.; Wadt, W. R. Ab Initio Effective Core Potentials for Molecular Calculations. Potentials for K to Au Including the Outermost Core Orbitals. *J. Chem. Phys.* **1985**, *82* (1), 299–310.
- (58) Casida, M. E. *Recent Advances in Density Functional Methods: Part I*; World Scientific: Singapore, 1995; Vol. 1.
- (59) Dreuw, A.; Head-Gordon, M. Single-Reference Ab Initio Methods for the Calculation of Excited States of Large Molecules. *Chem. Rev.* **2005**, *105* (11), 4009–4037.
- (60) Stratmann, R. E.; Scuseria, G. E.; Frisch, M. J. An Efficient Implementation of Time-Dependent Density-Functional Theory for the Calculation of Excitation Energies of Large Molecules. *J. Chem. Phys.* **1998**, *109* (19), 8218–8224.